Journal of Applied Polymer Science

WILEY

Applied Polymer SCIENCE

RESEARCH ARTICLE OPEN ACCESS

Characteristics of Polyurethane Pyrolysis—Experimental Investigations and Product Analyses for the Assessment of Chemical Recycling Potentials

Michael Zeller | Lea Wattenberg | Pratistha Shrestha | Aylin Hannemann | Ankh-Erdene Erdenepurev | Niklas Netsch | Britta Bergfeldt | Salar Tavakkol | Dieter Stapf

Institute for Technical Chemistry, Karlsruhe Institute of Technology, Karlsruhe, Germany

Correspondence: Michael Zeller (michael.zeller@kit.edu) | Salar Tavakkol (salar.tavakkol@kit.edu)

Received: 7 October 2025 | **Accepted:** 4 November 2025

Keywords: chemical recycling | degradation | gas chromatography | lab scale | polyurethane | pyrolysis | recycling | thermosets

ABSTRACT

Understanding polyurethane (PUR) decomposition is essential to promote the chemical recycling of plastic waste via pyrolysis. In this study, four representative polyurethanes were pyrolyzed in a lab-scale batch pyrolysis system to investigate their thermal decomposition characteristics. The solid, condensate and gas yields and the chemical composition of the product phases strongly depend on the structural PUR configuration and the pyrolysis temperature. In all cases, the condensate is the dominant product phase, exhibiting a broad compound spectrum, attributable to the urethane bond scission and the polyol backbone disintegration. The polyurethane monomer methylene diphenyl diisocyanate (MDI) is not detected. Up to 15 mass-% of the PUR is converted to the PUR monomer precursors 4,4′-methylenedianiline (MDA) and aniline. Secondary reactions, including MDI derivatization, are plausible. CO_2 is the main gaseous compound, accompanied by short-chain hydrocarbons and oxygenated compounds. Nitrogen retention in the solid phase indicates urethane bond involvement, while oxygen mainly migrates to the condensate and gas. This study provides in-depth information on PUR pyrolysis characteristics, laying the foundation for the development of circular PUR waste-to-chemical processes. Potentials and challenges for chemical recycling are highlighted. The necessity of further research on PUR co-pyrolysis, adequate compound separation, and product upgrading is emphasized.

1 | Introduction

The Sustainable Development Goals (SDG) set by the United Nations call for an innovative and conscious use of resources and energy, along with the sensible handling of waste materials [1]. As primary measures, the consumption of fossil-based products must decrease, and the reuse of materials is imperative. In addition, sustainable recycling routes for waste must be established. This applies in particular to plastic waste. Currently, the majority of plastic waste is landfilled, incinerated, or mismanaged, causing environmental pollution [2]. Generally, numerous recycling technologies are available that enable the closing of material cycles for specific waste fractions [3]. The establishment of an effective circular plastic economy is only possible through a combination of suitable and available technologies. For many plastic waste types, such as polyethylene, polystyrene, or polyethylene terephthalate, recycling processes are already established on a commercial scale [4–6]. Commonly, such processes are challenged by polymer aging, contaminants, and complex plastic mixtures [6, 7]. For polyurethanes (PUR), which make up 5.3% of the yearly polymer production [8], fewer effective technologies are available. PUR are manufactured from polyisocyanates and polyalcohols, which enables tailored properties and a broad application range. Based on their chemistry, PUR carry nitrogen and oxygen and are generally thermoset polymers. Typical applications are rigid and flexible foams, elastomers, coatings, and

adhesives [9]. Major PUR users are the automotive, furniture, and construction industries [10]. Hence, mechanical recycling of PUR and chemical recycling via solvolysis struggle with the complexity of PUR waste streams [11]. In mechanical PUR recycling, PUR wastes are often ground and used as fillers or adhesively rebonded without retaining their original product properties [12]. For solvolysis processes, which aim to recover polyols from PUR waste, significant effort is to be made to isolate the target products from the solvent and by-products [13]. It is evident that high-quality recycling of PUR is reasonable from an environmental perspective, and several environmental burdens can be avoided [14]. In the recent past, chemical recycling of plastics via pyrolysis has gained momentum due to its robustness and its applicability to a wide range of wastes [5, 15]. In pyrolysis, materials are subjected to thermal decomposition at elevated temperatures without additional oxidizer. Pyrolysis yields a combination of solid, condensed, and gaseous products that can potentially be reintroduced into existing chemical value chains [15]. In this way, pyrolysis can help to achieve circularity. As summarized in a review by Oenema et al. [16], the pyrolytic decomposition phenomena and the product spectrum of PUR have been investigated in small-scale experiments such as thermogravimetry (TGA) and Pyrolysis-Gas-Chromatography-Mass-Spectroscopy (Py-GC-MS). Herein, the initial decomposition of the urethane bonds in the polymer either produces the monomers isocyanate and polyol or an amine derivative of the isocyanate and CO_2 [17]. The cleavage of the polyol segments in the PUR occurs independently of the urethane bond scission. Due to the heterogeneous chemical structure of PUR polymers, a diverse product spectrum is evident. Small-scale experimental systems like TGA and Py-GC-MS are designed for minimal heat and mass transfer influence, and residence times are typically low. Furthermore, the evolved pyrolysis products are usually rapidly quenched, heavily diluted, and directly transferred to the respective analyzer. In contrast to a lab- or technical-scale pyrolysis system, the condensation of pyrolyzates is not intended, and no condensation unit is employed. Mkhize et al. [18] have demonstrated a significant influence of the pyrolysis system and the condensation unit on the yield and composition of pyrolysis products. Thus, it remains unclear if the dominant mechanisms of PUR pyrolysis on a small scale still define the decomposition on a technical scale. For product recovery on a technical scale, a condensation unit must be employed. It is thus likely that secondary reactions influence the product yields and composition. To assess PUR pyrolysis as a circularity-enabling technology, a thorough elucidation of valid pyrolysis mechanisms, recoverable product phases, and their composition is necessary. This information can only be partially provided by TGA and Py-GC-MS, requiring experimentation on a larger scale. However, such investigations at lab- or technical scale are scarce [19, 20]. In the presented work, the pyrolysis of four different PUR of representative composition is investigated in a lab-scale batch pyrolysis system. Pyrolysis products are collected, and mass balances are derived. The condensed and non-condensed products are analyzed with advanced quantitative GC techniques. Previously reported TGA and Py-GC-MS analyses of the identical polymers allow an estimation of scale phenomena [21, 22]. As a result, the derived mass balances and product yields allow an assessment of the influence of the PUR type and the process conditions on the pyrolysis. Subsequently, the chemical recycling potential of PUR can be evaluated.

2 | Materials and Methods

2.1 | Polyurethanes

The investigated polyurethane materials comprise a rigid foam (RPUF), a flexible foam (FPUF), a cast elastomer (CE), and a thermoplastic PUR (TPU). Each material is a representative of typical PUR applications. All materials were synthesized based on MDI as the uniform monomer. For RPUF and FPUF, polyether polyols were used in the formulation. Foaming was achieved by the addition of water. The added water reacts with the isocyanate to form carbon dioxide, inducing the foaming process. The foaming reaction further causes the formation of biurets and ureas. The formulations of CE and TPU are based on 1,4-Butanediol (BDO) and Polytetrahydrofuran (PTHF). Details on the sample composition are reported in Tables 1 and 2. The samples investigated in this work are identical to those from previous publications [21, 22]. No relevant amounts of mineral substances are contained in the PUR.

TABLE 1 | Composition of the model PUR investigated in the presented study.

	RPUF	FPUF	CE	TPU
Ingredient	**mass-%**	**mass-%**	**mass-%**	**mass-%**
Polytetrahydrofuran	—	—	77.6	Mass fraction not disclosed
Propylene oxide-based polyether-polyols	31.7	56.1	—	—
Ethylene oxide-based polyether-polyols	—	10.3	—	—
Sorbitol	7.2	—	—	—
Glycerol	4.1	1.6	—	—
MDI	56.3[a,b]	28.8[a,b]	20.3[a]	33.3[d]
1,4-Butanediol	—	—	2.0	Mass fraction not disclosed
Sum[c]	99.3	96.8	99.9	—

[a]The exact isomer composition is unknown.
[b]Sum of MDI and polymeric MDI.
[c]Difference to 100% includes non-disclosed additives and foaming agent water.
[d]Calculated from the nitrogen content of the elemental analysis.

2.2 | Lab Scale Pyrolysis Experiment

A lab-scale batch pyrolysis system was employed. The setup is displayed in Figure 1.

The pyrolysis system comprises mass flow controllers for nitrogen and argon dosing, a reactor placed in an electrically heated oven, a double tube condensation unit, and a gas collection unit. The reactor consists of a horizontal tube of 2.9 cm inner diameter and 5 cm length, which serves as the reaction chamber. Flushing gas was supplied via a vertical inlet tube welded to the horizontal section of the reactor. This inlet tube further accommodates a thermocouple, which was used to record the internal reactor temperature and control the oven. The pyrolysis products are swept out of the reactor to the condensation unit via a second vertical tube, welded to the opposing end of the horizontal section. The reactor unit attaches to the peripheral system components via compression ferrule fittings at the upper ends of the vertical tubes. All parts of the system between the gas inlet and the outlet of the condensation unit are made from stainless steel and connected via compression ferrule fittings.

TABLE 2 | Elemental composition of the model PUR investigated in the presented study.

Sample	RPUF mass-%	FPUF mass-%	CE mass-%	TPU mass-%
C	70.0	68.1	70.5	71.5
H	6.7	8.5	9.4	8.4
N	6.9	3.3	2.1	3.7
O (Difference to 100)	16.4	20.1	18.0	16.4

Before each experiment, the reactor, the connection pipes, and the condensation unit were weighed. Then, between 1.5 g and 4.5 g of sample was filled into the reactor via the gas inlet tube and distributed evenly in the horizontal section of the reactor. The reactor and condensation unit were sealed airtight and flushed with nitrogen for several minutes to ensure an inert atmosphere. The cooler of the condensation unit was set to −5°C. A mix of water and ethylene glycol was used as a coolant. The oven was then heated from ambient temperature to the desired pyrolysis temperature. After the heat-up phase, the reactor temperature was kept constant. The oven set temperature varied for different experiments between 450°C and 550°C. The total runtime of the experiment was set between 1 and 3 h. The long experimental runtimes were chosen to ensure complete

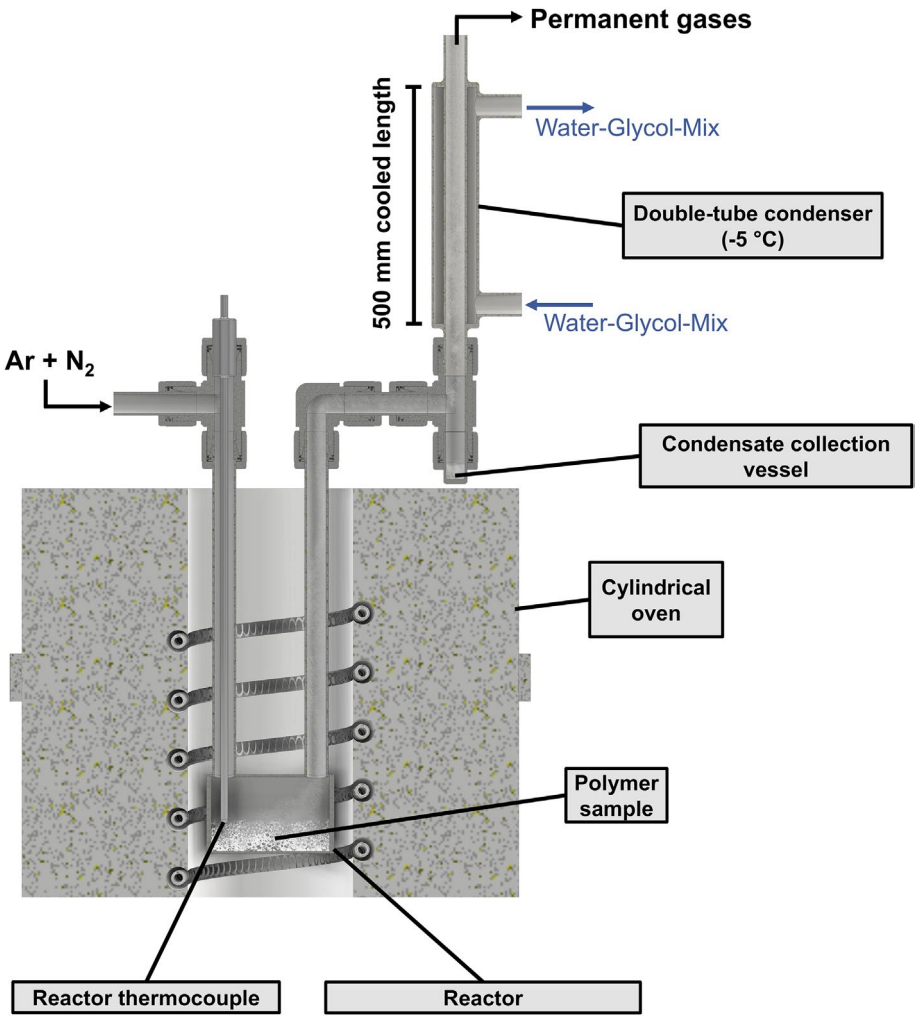

FIGURE 1 | Schematic drawing of the lab-scale batch pyrolysis system. [Color figure can be viewed at wileyonlinelibrary.com]

conversion of the polymer and non-volatile pyrolysis intermediates. The evolved pyrolysis vapors were constantly flushed to the condensation unit by a flushing gas flow of 50 mL min^{-1} consisting of nitrogen and argon in a defined ratio. Consequently, the residence time in the hot section of the system is independent of the total experimental runtime. The residence time amounts to approx. 15 s before the volatiles are quenched in the condensation unit. Non-condensable products of the pyrolysis were collected in a RESTEK Tedlar gas bag for analysis.

After the end of the experiment, the oven was switched off, and the reactor was removed from the oven to quench the pyrolysis. The system was then disassembled and weighed again. From the weight difference, the mass balance was derived. Products found in the transfer pipe from the reactor to the condenser, the condenser, and the connection tube to the gas bag were considered condensates. Material remaining in the reactor was registered as solid residue. The mass of the produced gas was calculated by difference. Thus, it comprises all potential losses and uncertainties. A refinement of the mass balance can be performed by inclusion of individually quantified gaseous products (see Section 2.3.4). After weighing, the condensation unit was disassembled, and the condensate was recovered and stored in vials. The system was then washed with Chloroform ($CHCl_3$) to remove residual products. Insoluble deposits in the reactor were burned off by heating the reactor with a gas burner in an air atmosphere. This procedure prevents product carryover to subsequent experiments. Each experiment was conducted at least twice, and mass balances were averaged. Exemplary temperature profiles of experiments with different isothermal temperature setpoints are reported in the Data S1.

2.3 | Product Analytics

2.3.1 | Elemental Analysis

Elemental Analysis of solid and condensed pyrolysis products was performed in a Leco TruSpec Micro. Approximately 1 mg of sample was used per analysis. All analyses were repeated at least twice.

2.3.2 | GC-MS

Condensate analyses were performed in an Agilent 6890 Gas chromatograph (GC) coupled to a 5973 Quadrupole Mass Spectrometer (MS) with a Restek RTX200MS column (30 m, 0.25 mmID, 0.25 μm film thickness). The samples were prepared by dilution with $CHCl_3$ in a ratio of 1:5 or 1:10. An automatic liquid sampler was employed for the injection of 1 μL of the diluted sample per analysis. The split/splitless inlet was heated to 270°C and flushed with Helium at a pressure of 75 kPa. The split ratio was set to 60:1 with a total flow of 87 mL min^{-1}. During the analysis, the oven temperature was initially held constant at 40°C for 5 min. Subsequently, the oven temperature was ramped at 2°C min^{-1} to 150°C and at 5°C min^{-1} from 150°C to the final temperature of 300°C. An isothermal dwell time of 10 min was used. The total runtime of the analysis was 100 min. The MS was operated in scan mode. The MS transfer line was heated to 250°C, and the ion source was heated to 230°C. The quadrupole temperature was 150°C.

The presented method is the result of an extensive method development. Several solvents and method parameter variations were tested to optimize solvent capability while minimizing coelution with substances of particular interest and maintaining acceptable peak shapes. Due to the heterogeneity of the condensates and the multitude of compounds to be separated, plenty of effort was put into this. The expected compounds of interest, MDI and MDA, exhibit high boiling points above 350°C. Consequently, the inlet temperature was initially set to the highest possible temperature of 320°C to promote the evaporation of high-boiling analytes. At this temperature, unsatisfactory chromatograms were obtained, which were attributed to secondary pyrolysis and recombination. Therefore, the inlet temperature was lowered in a stepwise method adaptation to 270°C.

The chromatograms were evaluated using the postprocessing software Lablicate OpenChrom. For the MS spectrum library search, the NIST 17 spectral database was employed. Only peaks with > 80% match factor were considered identifiable.

Calibration was performed by injection of reference mixes. Calibration mixes with target analyte concentrations of 1.0, 2.5, 5.0, 7.5, and 10 mg ml^{-1} were injected. During the calibration, reliable evaporation of MDA with the previously defined method parameters was verified. Subsequently, calibration formulae were derived via regression. The calibration curves and formulae of aniline and 4,4′-MDA are displayed in Figure S1. The coefficients of determination for aniline and 4,4′-MDA exceed $R^2 > 0.9995$. For aniline, with a boiling point of 184°C, no discrimination due to the inlet temperature is expected. As both calibration curves exhibit equally high coefficients of determination and linearity, reliable quantification of MDA is to be assumed. The GC-MS was serviced and recalibrated multiple times over the course of the presented study to ensure accurate quantification.

2.3.3 | GCxGC-FID-MS

Two-dimensional gas chromatography (GCxGC) was used for a detailed, qualitative analysis of the condensed pyrolysis products. Per analysis, 1 μL of sample diluted in $CHCl_3$ was injected into a Multi Mode Inlet (MMI). The evaporated sample was flushed through the system by helium carrier gas. A non-polar Agilent DB-5MS (20 m, 0.18 mm i.d., 0.18 μm film thickness) was installed as the first column, separating the analytes according to their boiling point. A reversed flow modulator performed modulation and injection into the second separation column. The second employed column was a Trajan BPX50 (5 m, 0.25 mm i.d., 0.25 μm film thickness) of intermediate polarity. It retains compounds according to their polarity. After elution from the second column, the gas stream was split and fed to the MS and the flame ionization detector (FID). The obtained data consist of the retention times on the first and second columns and the signal intensity of the respective detector. Thus, the data is three-dimensional and is usually displayed as a color plot. Signal peaks are referred to as blobs in 2D chromatography.

Correspondingly, the abundance of a substance in the analyzed sample is reported as blob volume instead of peak area.

Method development for GCxGC was performed in analogy to the GC-MS method development. For optimal analyte evaporation, the inlet temperature was set to the maximum temperature of 400°C. Unfortunately, secondary pyrolysis and interactions of the analytes with the solvent $CHCl_3$ were evident. Consequently, the method temperature was lowered. In contrast to the split/splitless inlet of the GC-MS, the MMI of the GCxGC still allowed higher inlet temperatures without secondary pyrolysis. An inlet temperature ramp from 300°C to 340°C was used. Extended details of the analysis method are listed in Table S1. The GCxGC system features a high resolution and enabled compound group specific product characterization and the identification of main compounds.

2.3.4 | GC-TCD-Fid-MS

An Agilent 8890 GC with a configuration customized by Teckso GmbH was employed for the analysis of non-condensable pyrolysis products. It is equipped with an automatic gas sampling unit, two sample loops, multiple switching valves, an additional isothermal column oven, and multiple columns connected via Deans switches. A thermal conductivity detector (TCD), a flame ionization detector (FID), and an Agilent 5977C MS are employed. This setup enables high separation efficiencies and detection and identification of crucial products. The employed setup and method were described in detail in a previous publication [23]. The system was calibrated with calibration gases of defined concentrations. Volatiles, which cannot be supplied from gas cylinders, were fed to the system in $CHCl_3$ or octane solution. This procedure was validated with substances that are available in both gaseous and liquid form.

2.3.5 | ATR-FTIR

Attenuated total reflection Fourier-transform infrared spectroscopy (ATR-FTIR) analyses of the solid pyrolysis products were performed on a Bruker Optics Tensor II spectrometer equipped with a deuterated triglycine sulfate (DTGS) detector and a Golden Gate ATR cell with a diamond crystal (Specac LTD). The spectra acquisition range was 400–4000 cm^{-1} with 64 scans and a spectral resolution of 2 cm^{-1}. Acquisition and evaluation of the spectra were performed using OPUS 8 software.

3 | Results & Discussion

3.1 | Mass & Element Balances

The mass balances obtained from experiments at 450°C, 500°C, and 550°C are displayed in Figure 2. The yield of the different product fractions is strongly feedstock-dependent. For all investigated PUR, the condensate is the dominant product phase. Condensate yields range between approximately 60 and 75 mass-%. The maximum amount of condensate was obtained from CE pyrolysis with an isothermal dwell temperature of 550°C, with 75.8 mass-%. The condensate yield of CE is the highest of the four investigated PUR. The yields of RPUF, FPUF, and TPU are similar to each other. TPU pyrolysis with an isothermal dwell temperature of 450°C yields the lowest amount

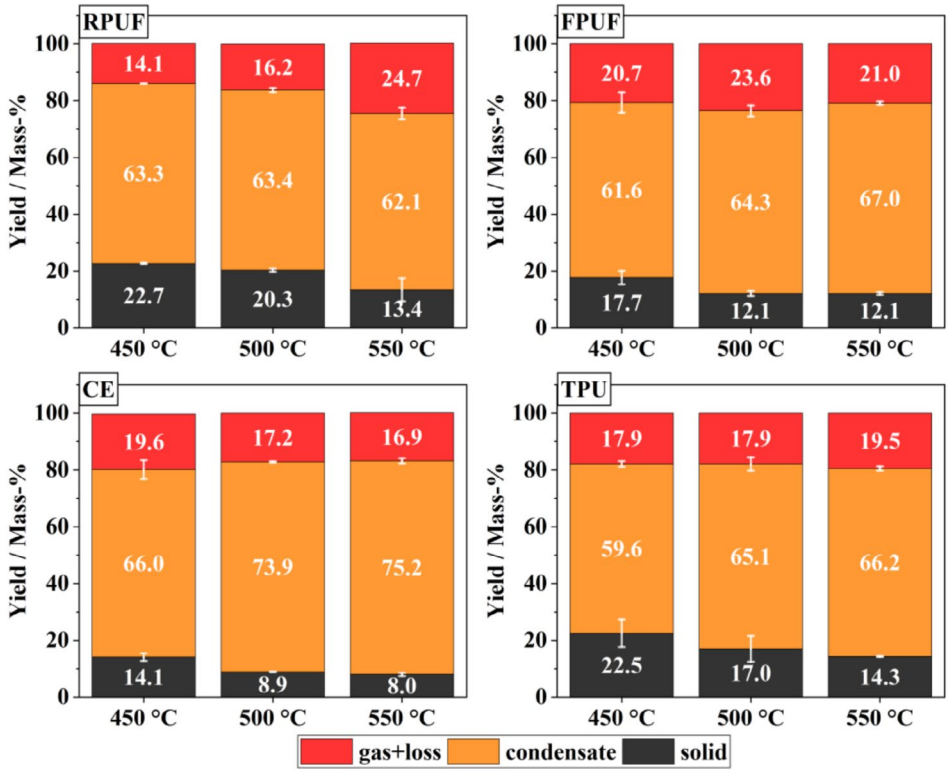

FIGURE 2 | Mass balances from lab-scale experiments (450°C, 500°C, and 550°C, and 3 h total runtime). Average of at least two experiments per setpoint. [Color figure can be viewed at wileyonlinelibrary.com]

of condensate with 59.6 mass-%. With increased temperature, the pyrolysis of FPUF, CE, and TPU yields a higher fraction of condensate. The condensate yield from RPUF pyrolysis remains virtually constant with increased temperature. An increase in isothermal dwell temperature leads to a reduction of solid residue for all PUR. RPUF pyrolysis at 450°C isothermal temperature yields 22.7 mass-%, which is the highest amount of residue. For CE pyrolysis at 550°C, the lowest solid yield is observed with 7.6 mass-%. The yield of pyrolysis gas is marginally influenced by the reactor set temperature. It must be acknowledged that the gas yield and the balance loss are reported in combination and are consequently subject to a higher degree of uncertainty. The pyrolysis gas yield and composition are resolved in greater detail by the GC-TCD-FID-MS analyses discussed in Section 3.2.3.

Compared to findings from TGA reported in previous publications [21, 22], an increase in solid formation is evident for FPUF, CE, and TPU. A comparison of solid yields from TGA and the lab-scale experiments presented in this work is given in Table 3.

The RPUF solid yield is comparable in both experimental setups, TGA and lab-scale pyrolysis. FPUF, CE, and TPU lab-scale pyrolysis yields significantly more solid residue. In TGA, evolving volatiles freely evaporate from the crucible and are immediately heavily diluted by the flushing gas. The rapid discharge from the hot zone of the oven further suppresses secondary reactions. In contrast, the ratio of sample to carrier gas flow is much higher in the lab-scale system. Hence, the evolving pyrolysis vapors are less diluted, which may promote secondary reactions and subsequent solids formation. Additionally, the geometry of the reactor and the packing of the PUR may lead to a stronger influence of material transport and intensified contact of the pyrolysis intermediates and products with the reacting polymer. Regarding the temperature dependency of the solid yields, one may conclude that, effectively, a reactive distillation occurs. The pyrolysis products are of such high boiling points that they cannot volatilize and escape from the reactor at the respective reactor temperature. Consequently, they are classified as solids in the employed setup. Previously reported isothermal TGA has shown that intermediate temperature isothermal pyrolysis does not lead to a significantly increased solids formation, compared to purely dynamic TGA [21]. Grittner et al. [19] have investigated fluidized bed pyrolysis of a rigid PUR foam. They registered a solid yield of 2.3 and 4.9 mass-% at pyrolysis temperatures of 700°C and 800°C, respectively. Additionally, they report a high-boiling aromatic tar fraction, rich in N and O, of 13.5 and 8.2 mass-%. The char yield is significantly lower compared to the experiments presented in this work. The sum of tar and solids is, in turn, comparable to the solid yields obtained in this work. This underlines the theory of reactive distillation as higher system temperatures appear to lead to lower amounts of residue. In the system presented in this work, the comparatively low temperatures presumably lead to incomplete separation of coke and tar. Hence, an elevated reaction temperature may decrease the yield of solid products.

TABLE 3 | Solid yields from TGA [21] and lab-scale experiments.

Material	Solid yield from TGA[a] [21] mass-%	Solid yield from lab-scale pyrolysis[b] mass-%
RPUF	14	13.4
FPUF	6	11.3
CE	-[c]	8.0
TPU	-[c]	14.3

[a]Final temperature of 900°C.
[b]Final temperature of 550°C.
[c]No significant solid yield was detected.

Figure 3 shows the elemental migration into solid, liquid, and gaseous product phases of the respective PUR derived from the mass balancing and elemental analysis. The methodology is given in the SI.

The majority of carbon, hydrogen, and nitrogen migrates to the condensed fraction. Pyrolysis, as conducted in this study, does not lead to a coordinated discharge of certain elements to certain product phases. If no direct waste-to-polymer recycling can be achieved, feedstock recycling via reintroduction of pyrolysis products into chemical industry processes is desired. High levels of contaminants like nitrogen, oxygen, or halogens in the pyrolysis condensate limit prospective outlet processes. Processes like steam crackers, that predominantly rely on fossil feedstocks, set strict feedstock specifications. Catalytic processes may be severely harmed by heteroatoms in a pyrolysis-based feedstock [24]. Hence, pyrolysis mechanisms that intrinsically lead to the migration of heteroatom contaminants to the permanent gas phase or the solid phase are beneficial. The presented observations for PUR stand in contrast to, for example, the pyrolysis of polyvinyl chloride (PVC). In the primary step of PVC pyrolysis, chlorine is predominantly released into the gaseous phase as hydrogen chloride (HCl), leading to a mostly dehalogenated condensate phase [25]. The formation of hydrogen chloride poses individual challenges due to its corrosiveness and potential chlorine migration to the condensate, which can be mitigated by, for example, the use of mineral additives [26] or metal sorbents [27].

For the investigated PUR and the applied experimental system and parameters, pyrolysis does not aid in oxygen or nitrogen unloading. While both the pyrolysis temperature and the type of PUR influence the product distribution, condensed products consistently make up the largest product fraction. The heterogeneous composition of the PUR is reflected in the pyrolysis products, requiring further detailed analysis of all product phases.

3.2 | Pyrolysis Products Analysis

3.2.1 | Solid Pyrolysis Products

The elemental composition of the obtained pyrolysis solids is reported in Table 4.

The elemental analysis reveals that the pyrolysis solids mainly consist of carbon. Significant amounts of nitrogen and oxygen are retained in the pyrolysis solids. In relation to the feedstock (see Table 2), the nitrogen content is increased. This hints at the nitrogen-carrying segments of the PUR as crucial participants

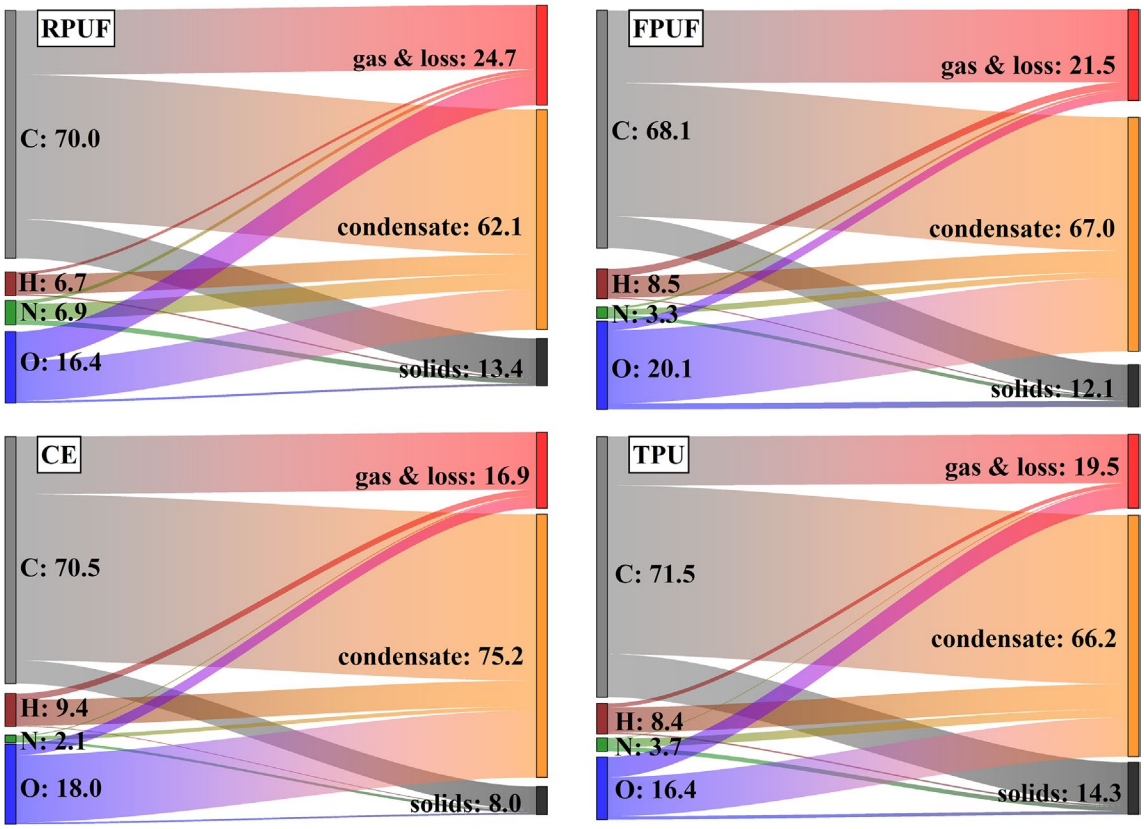

FIGURE 3 | Element migration during lab-scale PUR pyrolysis (550°C and 3 h total runtime). [Color figure can be viewed at wileyonlinelibrary.com]

TABLE 4 | Elemental composition of pyrolysis solids from RPUF, FPUF, CE, and TPU lab-scale pyrolysis (550°C and 3 h total runtime).

Material	C	H	N	O (difference)
RPUF	81.9	2.9	10.4	4.8
FPUF	75.0	2.9	8.2	13.9
CE	82.7	2.5	8.3	6.5
TPU	82.3	2.6	8.5	6.6

in the solid formation mechanism. For RPUF, this comprises the urethane bonds and other nitrogen-carrying bonds such as ureas and biurets, likely formed during foaming. In the case of CE and TPU, no foaming procedure was performed, leaving urethanes as the sole nitrogen-carrying bonds in the polymer. The solids formation from the urethane bond is thus evident. Compared to the feedstock, the oxygen content is lowered for the solids. Thus, the incorporation of significant amounts of the polyol segments in the solids is unlikely. The oxygen content cannot be determined directly and is calculated by difference. Hence, the reported values are of greater relative uncertainty. Still, the amount of oxygen in the solids residues cannot be neglected. One can assume that large polyol fragments with boiling points that exceed the pyrolysis temperature are formed.

The obtained solids were analyzed by ATR-FTIR. The results are displayed in Figure 4.

For TPU, the C—H stretching absorption bands around 2900 cm^{-1} may originate from PolyTHF segments incorporated into the solids. This theory is supported by the intense band at 1103 cm^{-1} belonging to the C—O—C stretching vibration [28]. This band is clearly attributable to the PTHF backbone. The sharp C—O—C stretching band and the C—H stretching bands around 2900 cm^{-1} are absent in the spectra of the RPUF, FPUF, and CE solids. No PTHF was used for RPUF and FPUF synthesis. Hence, the absence of the aforementioned bands is conclusive. In CE pyrolysis, the PTHF backbone appears to either not participate in solids formation or be derivatized.

The intense band at 1580 cm^{-1} present in all samples is attributed to aromatic C=C stretching. The band at 748 cm^{-1}, belonging to aromatic out-of-plane C—H bending, further indicates the presence of aromatic ring structures in all solids. The 1435 cm^{-1} band is attributed to aromatic ring stretching as well. The intense absorption in the region 1250–1360 cm^{-1} hints at the presence of amines [28]. This region overlaps with the C—O stretching band at ca. 1100 cm^{-1}. The formation of aromatic amines during the pyrolysis of PUR is abundantly reported in the literature [16]. It is conclusive that the aromatic amines produced during pyrolytic decomposition undergo secondary reactions and form oligomers and secondary polymers, with boiling points that exceed the pyrolysis temperature, as discussed in Section 3.1. Hence, these compounds are classified as solids. In FPUF, TPU, and CE pyrolysis, the polyol backbone appears to be partially incorporated into the solids. This is supported by the, compared to RPUF, higher content of oxygen determined by the elemental analysis. Previously reported findings from segmented TGA

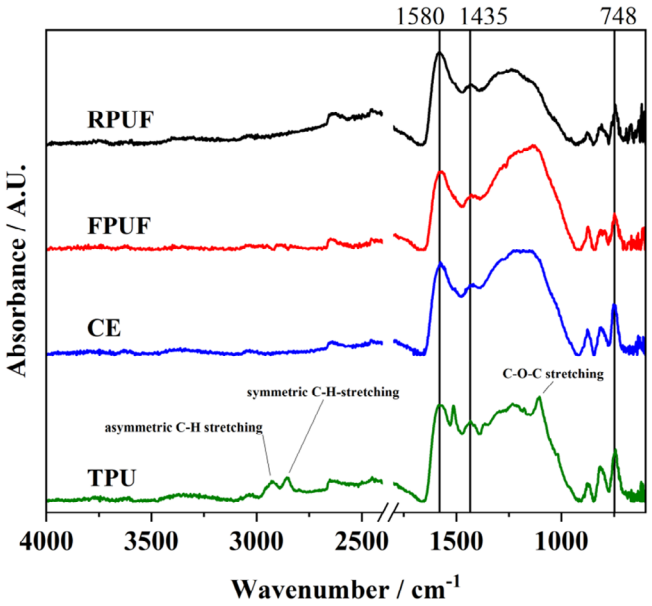

FIGURE 4 | ATR-FTIR analyses of RPUF, FPUF, CE, and TPU solids (550°C and 3 h total runtime). [Color figure can be viewed at wileyonlinelibrary.com]

experiments match the observations made at lab-scale concerning the retention of nitrogen in the solid [21].

3.2.2 | Condensed Pyrolysis Products

The condensed pyrolysis products were analyzed by GCxGC-FID-MS. GCxGC provides detailed and comprehensive qualitative product analysis. GCxGC chromatograms of PUR condensates are displayed in Figure 5 for RPUF, Figure 6 for FPUF.

Figure 7 for CE, and Figure 8 for TPU. Experimental details are given in the Data S1.

The two-dimensional chromatographic separation of the pyrolysis condensate reveals different substance groups within the condensate. After first-dimension separation according to boiling point, the second-dimension separation according to polarity allows isomers and substances with different functional groups to be distinguished, which drastically increases the identification potential compared to one-dimensional GC [29]. Substance groups identified in all investigated PUR condensates

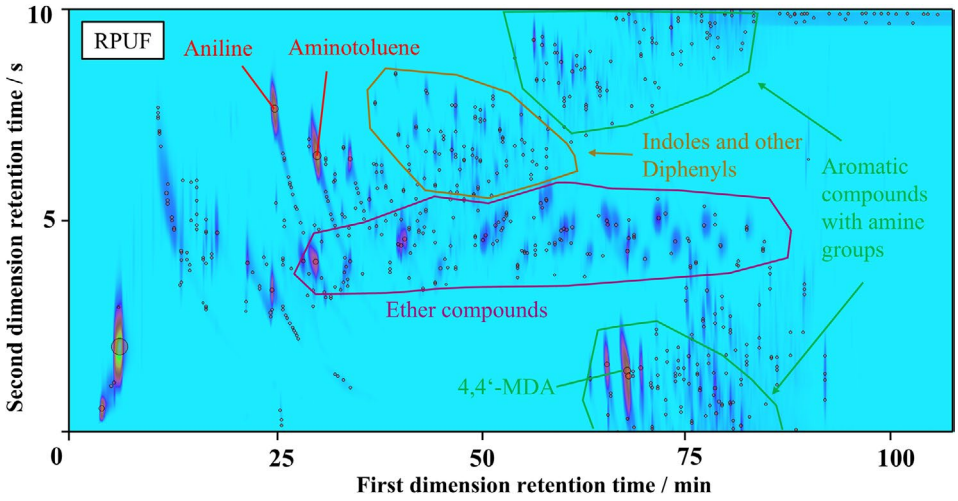

FIGURE 5 | GCxGC chromatogram of RPUF condensate from lab-scale PUR pyrolysis. [Color figure can be viewed at wileyonlinelibrary.com]

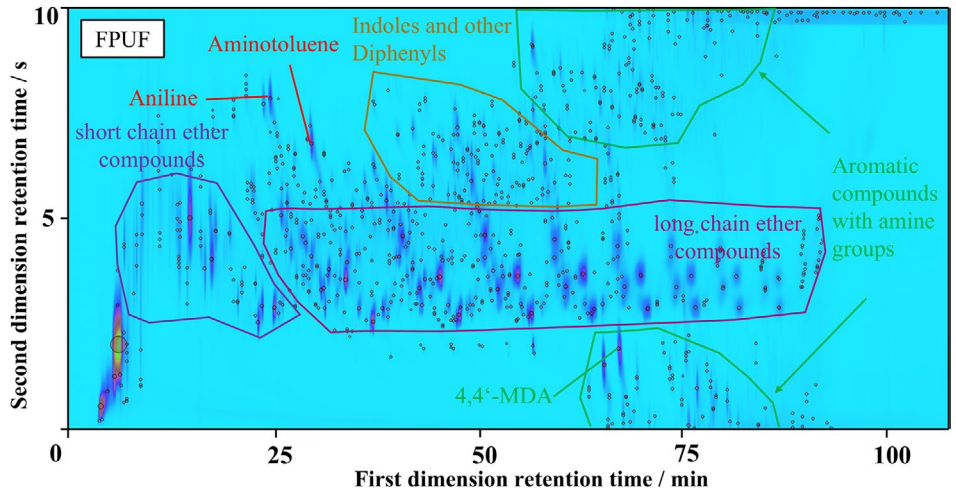

FIGURE 6 | GCxGC chromatogram of FPUF condensate from lab-scale PUR pyrolysis. [Color figure can be viewed at wileyonlinelibrary.com]

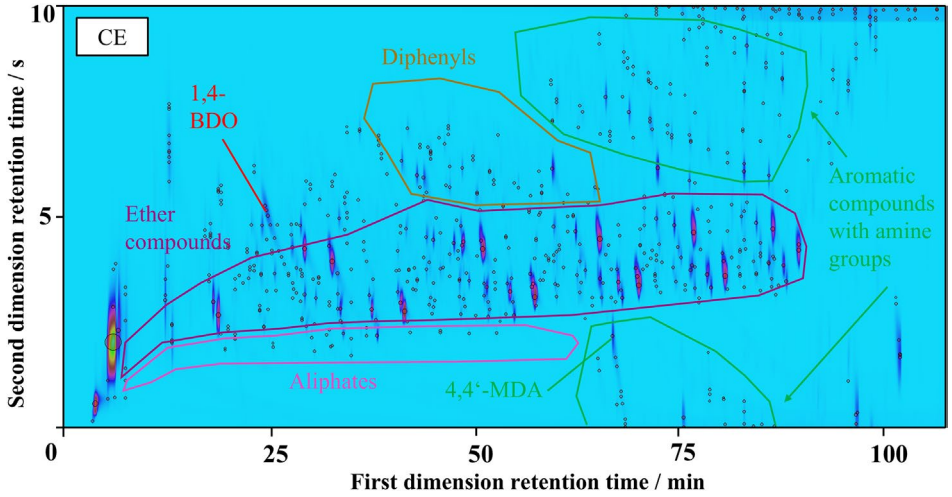

FIGURE 7 | GCxGC chromatogram of CE condensate from lab-scale PUR pyrolysis. [Color figure can be viewed at wileyonlinelibrary.com]

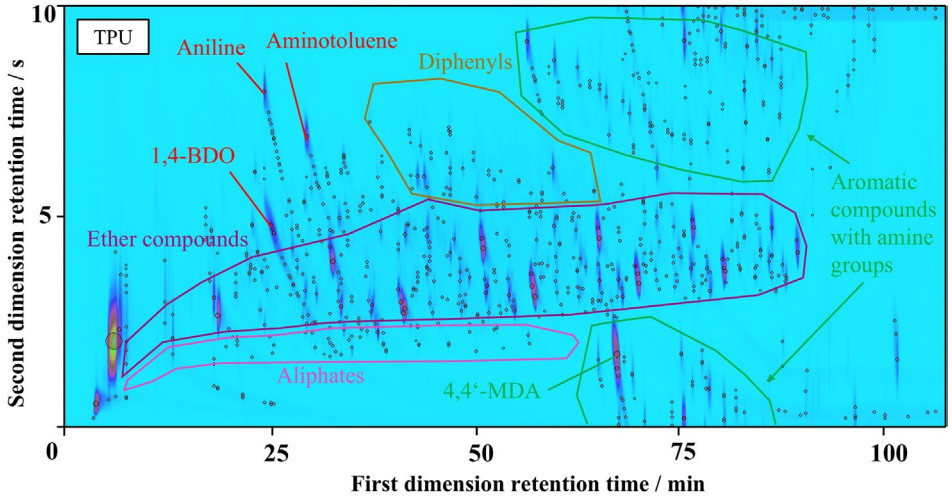

FIGURE 8 | GCxGC chromatogram of TPU condensate from lab-scale PUR pyrolysis. [Color figure can be viewed at wileyonlinelibrary.com]

are ether compounds and aromatic amines. These substance groups reflect the heterogeneous molecular structure of the original polymers. 4,4′-MDA is detected in all condensates and is accompanied by various other aromatic compounds carrying amine groups in the first-dimension retention time region between approximately 60 and 90 min. The aromatic amine region extends to higher retention times than that of 4,4′-MDA, which hints at larger molecules with higher boiling points. Mostly, these compounds cannot be definitively matched to a certain compound via the NIST MS spectral library, but can be classified by characteristic markers of certain mass-to-charge (m/z) ratios. For RPUF, the abundance of high-boiling aromatic amines is especially high, as evident from Figure 5. Since polymeric MDI was used for RPUF synthesis, a comparatively broad distribution of aromatic amines in the pyrolysis condensate is conclusive. The presence of these compounds, especially for RPUF, may also be interpreted as secondary scission or recombination during or after pyrolysis. Additionally, indoles and other nitrogen-carrying aromatics and cyclic compounds were detected, which are also likely derivatives of the urethane bond decomposition products. With aniline and aminotoluene, further aromatic amines are detected in the RPUF, FPUF, and TPU condensate. These compounds are likely formed from the scission of 4,4′-MDA and other aromatic amines with higher boiling points. The abundance of 4,4′-MDA and its derivatives is especially low in the CE condensate, while aniline and aminotoluene are not detected entirely. As the CE formulation contains the lowest amount of MDI of the investigated PUR, this observation is conclusive. For FPUF, CE, and TPU, the derivatization of urethane bond scission products appears to play a subordinate role. It is striking that isocyanate compounds are not detected in either of the PUR condensates. Nishiyama et al. [30] have found MDA, MDI, and MDI derivatives with amine and isocyanate groups during temperature-dependent pyrolysis of segmented PUR in a Py-GC-MS system. They have proven that higher temperatures favor the decomposition to amines over the depolymerization to isocyanates. Consequently, overlapping depolymerization and derivatization processes are likely to occur during the dynamic pyrolysis experiments presented in this work. Hence, isocyanates and amines are likewise expected in the condensates. The absence of MDI and the simultaneous presence of various aromatic amines and MDA derivatives strongly hints at an influence of secondary reactions on the product spectrum, which is not observable on Py-GC-MS scale. For TPU, a predominance of the depolymerization mechanism towards MDI formation was proven in a previous publication

using Py-GC-MS [21]. The presence of 1,4-BDO in the CE and TPU condensates further emphasizes the influence of secondary reactions on the product spectrum. The regeneration of the chain extender 1,4-BDO hints at depolymerization as the initial pyrolytic mechanism instead of a direct formation of an amine group, an olefin, and CO_2. Therefore, the simultaneous occurrence of MDA and 1,4-BDO strongly suggests a derivatization of initially formed MDI. Similar observations of parallel occurrence of 1,4-BDO and CO_2 as an indicator of the urethane derivatization mechanism were made by Herrera et al. [31]. RPUF and FPUF are synthesized without 1,4-BDO, which explains its absence in these condensates.

The wide variety of lower molecular weight aromatic amines is likely the result of secondary pyrolysis of MDA and MDI. The detected aromatic amines with retention times higher than MDA might originate from the recombination of MDI with MDA or its derivates. Eschenbacher et al. [32] have conducted pyrolysis of rigid and semirigid PUR in Py-GCxGC-MS at 600°C. These polymers are comparable to the RPUF and FPUF investigated in this study. They have detected MDA as the main nitrogenated product which is attributed to the direct derivatization of the urethane bond. Few other nitrogen-containing compounds such as methylquinoline, 1-benzyl-1H-pyrrole and aromatic and aliphatic nitriles are detected. Aromatic amines other than MDA are not discussed by the authors. Hence, a minor influence of secondary scission reactions and recombination seems apparent, as expected from a micro-pyrolysis experiment. In contrast, the analyses presented in this work strongly hint at alteration of the product spectrum by secondary reactions, which is attributable to scale effects.

The second prominent substance group detected in all four condensates is ether compounds. The ether compound region is widely spread between approximately 5 min and approximately 90 min along the first dimension. The polyol backbone likely undergoes radical chain scission to form the detected compounds in a broad chain length distribution [33]. The blobs in the ether region of FPUF share common ions of m/z 43, 45, 59, and 87, which are characteristic for ethers [34]. The boiling point and thus the retention time on the first dimension vary widely. Since the formed ethers are expected to be of very similar chemical composition, their retention time on the second column is constant. Thus, the horizontal orientation of the ether region is conclusive. This further supports the hypothesis of a chain-length distribution, similar to the typical product distribution of polyolefin pyrolysis [35, 36]. Eschenbacher et al. [32] report a broad distribution of ethers and oxiranes from the pyrolysis of rigid and semi-rigid PUR foams, which agrees well with the presented findings. Contrary to the urethane bond scission discussed above, the polyol backbone scission apparently produces a wide variety of compounds, even at a small scale, with an assumed minor influence of secondary reactions. Thus, the polyol scission products are intrinsically more diverse. This may be attributed to the radical decomposition mechanism [33]. The spectrum of oxygenated compounds in CE and TPU condensate is notably different from RPUF and FPUF. The distribution and the MS fingerprints of the blobs in the ether region of CE and TPU are clearly distinguishable from those of RPUF and FPUF condensate, so a difference in the pyrolytic decomposition of the polyol segments is apparent. The PTHF used as polyol in CE and TPU cleaves to form compounds with different characteristics compared to the polyether polyols used in the RPUF and FPUF formulations. The monomer tetrahydrofuran (THF) is a plausible product of PTHF pyrolysis. Since the retention time of THF in the employed system overlaps with that of the solvent $CHCl_3$, the presence of THF in the condensate cannot be confirmed by the condensate analysis.

Another notable difference between CE and TPU condensates compared to RPUF and FPUF condensates is the presence of aliphatic compounds. It is plausible that these are formed from the scission and recombination of the polyol backbone. The polyols used for RPUF and FPUF consist of shorter carbon chains that are interrupted by ether bonds more often. This may be the cause of the non-existent formation of aliphatics.

GC-MS was used for the quantification of aniline and 4,4′-MDA as compounds of particular interest. The obtained yields are reported in Table 5.

The aniline and MDA yields differ strongly in dependence on the employed feedstock. The MDA yields range between approximately 1.0% of the initial sample mass for CE and approximately 11% for RPUF. The aniline yields show the same tendency, with abundances below the detection limit for CE and a maximum of 4.7% for RPUF pyrolyzed at 500°C. The yield of aniline and MDA can be correlated with the amount of MDI used in the PUR formulation and, consequently, with the amount of urethane bonds in the polymer. A significant temperature dependency of the obtained yields is not observed in the lab-scale experiments. For the investigated polymers, the degradation of the urethane bond is generally known to commence at temperatures above approximately 300°C [16] and has been confirmed for the investigated polymers via TGA [21, 22]. In the presented lab-scale experiments, the pyrolysis temperatures exceed the urethane bond decomposition temperature. Therefore, a full initial decomposition of the urethane bonds in the polymer can be expected. This does not imply a full volatilization and transfer of the urethane bond scission products to the gaseous and condensed product phase. The pyrolysis solids analysis presented above underlines this. Due to the dynamic design of the experiment, the polymer experiences similar temperature profiles regardless of the final isothermal temperature, as displayed in Figure S1. The pyrolytic decomposition commences during the dynamic stage of the experiment, and the evolved products are continuously removed from the reactor. This may explain the weak influence of the final isothermal temperature on the observed aniline and 4,4′-MDA yields. Grittner et al. [19] report comparatively low aniline yields from pyrolysis experiments with polyether-based PUR foam in a fluidized bed reactor at 0.5 kg h^{-1}. A decrease from 0.9 mass-% to 0.6 mass-% is noted with an increase in pyrolysis temperature from 700°C to 800°C. In contrast, an increase in aromatics yield from 3.6 to 10.7 mass-% is reported. These findings hint at a pronounced influence of continued scission reactions that lead to denitrogenation and further derivatization of the primary and secondary pyrolysis products, such as MDA and aniline. The lower pyrolysis temperatures in the presented study appear beneficial to the production of the potential value products MDA and aniline. Herrera et al. [31] have found no influence

TABLE 5 | Aniline and 4,4′-MDA yields in mass-% of the initial sample mass, obtained from experiments at different isothermal temperatures.

	450°C		500°C		550°C	
	Aniline-Yield	**4,4′-MDA Yield**	**Aniline-Yield**	**4,4′-MDA Yield**	**Aniline-Yield**	**4,4′-MDA Yield**
	mass-%	**mass-%**	**mass-%**	**mass-%**	**mass-%**	**mass-%**
RPUF	4.0	10.8	4.7	10.7	4.4	8.3
FPUF	0.3	1.6	0.3	1.7	0.3	2.1
CE	-[a]	1.0	-[a]	0.6	-[a]	1.1
TPU	0.3	7.9	0.4	4.3	0.3	5.5

[a]Compound not detected.

of the polyol structure on the formation of polycyclic aromatic hydrocarbons during pyrolysis, which further emphasizes the derivatization of urethane bond scission products at elevated temperatures.

The results in Table 5 underline that the condensate composition is elucidated to only a minor extent by main component quantification. The substance grouping presented in Figures 5–8, lays the groundwork for a facilitated quantitative assessment of pyrolysis condensates.

3.2.3 | Gaseous Pyrolysis Products

The results of the gas analyses via GC-TCD-FID-MS are reported in Table 6.

The gaseous product spectrum is dominated by CO_2 for all investigated PUR. The further gaseous products detected in significant abundance depend on the PUR type.

In RPUF pyrolysis gas, the short-chain hydrocarbons methane, ethane, ethene, propane, and propene are detected. The propene yield is of the highest proportion among the named substances, with approximately 0.9 mass-%. Hydrocarbons of higher chain length are not detected in significant amounts except for benzene, toluene, and m-xylene.

The gaseous product spectrum of FPUF is similar to that of RPUF. C_1 to C_3 hydrocarbons are the most abundant products besides CO_2. Additionally, propanal, acetone, and ethanal are detected but not quantified.

The gaseous product phase of CE and TPU pyrolysis contains THF. From the PTHF polyol backbone of these polymers, the formation of THF is conclusive. The majority of the formed THF is expected in the condensed phase. Due to the vapor–liquid equilibrium and non-ideal precipitation in the condenser, a fraction of products with boiling points exceeding the condenser temperature remains in the gas phase. As the $CHCl_3$ retention time overlaps with that of THF in GC-MS, it cannot be detected in the condensed phase. The detection of THF in the non-condensed product analysis proves the formation of monomers from PTHF. Further products of significant abundance in the CE and TPU pyrolysis gas are propanal, butanal, toluene, xylene, and ethanal. Saturated and unsaturated hydrocarbons of chain lengths C_1 to C_8 are found. The most abundant alkane compound is n-butane. The absence of C_3+ hydrocarbons and THF in the pyrolysis gas of RPUF and FPUF hints at the polyol backbone as the determining factor for the gas composition. The polyether polyols used for RPUF and FPUF are synthesized from ethylene oxide and propylene oxide. In these polyols, the repeating unit consists of a maximum of three carbon–carbon bonds, interrupted by an ether bond. It is thus conclusive that no hydrocarbons of higher chain length appear in the pyrolysis gas. In contrast, the PTHF backbone of CE and TPU carries four carbon–carbon bonds interrupted by ether bonds. Butane is among the most abundant compounds in the gas phase. Its formation from the polyol scission is conclusive. The appearance of longer-chained saturated and unsaturated hydrocarbons hints at recombination reactions of products from the radical chain scission mechanism of the PTHF [33]. The gaseous product composition is consistent with the condensed product composition regarding hydrocarbon formation. Aldehydes and further oxygenated compounds also likely form from the polyol decomposition.

Due to the integral collection method via gas bags employed in this work, no time- or temperature-resolved gaseous product evolution can be reported, as performed in TG-FTIR in previous work. Nonetheless, the results of the GC-TCD-FID-MS analysis generally match the previously reported product spectrum from TG-FTIR [22]. The carbon dioxide yields from PUR pyrolysis in TG-FTIR are given in Table 6. The CO_2 yields from the lab-scale pyrolysis presented in this work show only slight deviation from the TG-FTIR yields. On a lab scale, the pyrolysis of CE and TPU yields slightly more CO_2 than in TG. It is assumed that the predominant source of CO_2 is the scission of the urethane bond via six-membered ring transfer, displayed in Scheme 1b.

This mechanism yields an amine group, a C=C double bond, and CO_2. Additionally, urethane scission via depolymerization to isocyanate and alcohol group occurs as shown in Scheme 1a. For TPU, both mechanisms were proven previously [21]. Consequently, the depolymerization reaction lowers the CO_2 yield. The increase in CO_2 on lab scale may be due to the increased residence time and lower dilution of the pyrolysis products in the reactor. It is plausible that recombination reactions of formed isocyanates and alcohols occur, which in turn decompose via the six-membered ring transfer mechanism to amine, CO_2, and olefin. All three of these

TABLE 6 | Gaseous product species yields in % of the initial sample mass determined via GC-TCD-FID-MS (550°C and 3 h total runtime), and TG-FTIR CO_2 yields in % of the initial sample mass reported from Zeller et al. [22].

Material	CO_2 mass-% (Zeller et al. [22])	CO_2 mass-%	Ethane mass-%	Ethene mass-%	Propane mass-%	Propene mass-%	Butane mass-%	Butene mass-%	i-Butene mass-%	Tetrahydrofuran mass-%
RPUF	12.0	11.4	0.2	0.03	0.1	0.9	0.02	0.01	0.01	Not detected
FPUF	4.0	3.6	0.3	0.2	0.7	2.3	0.02	0.02	0.02	Not detected
CE	3.2	4.4	0.4	0.4	0.9	0.2	2.6	0.2	0.01	0.4
TPU	5.3	7.7	0.3	0.3	0.4	0.2	1.37	0.2	0.2	1.2

decomposition products are detected in the condensed and non-condensed products on lab scale. In TG-FTIR, secondary reactions are suppressed more strongly, which is expected to favor depolymerization. Hence, the CO_2 yield is lower in this case. Overall, the depolymerization mechanism plays a subordinate role on lab scale, leading to higher CO_2 yields in comparison to the TG-FTIR. Additionally, one can assume minor formation of CO_2 from the PTHF backbone [37], which further increases the yield and the observed difference between TG-FTIR and lab scale. RPUF and FPUF generally appear to favor the six-membered ring transfer mechanism. For this reason, the yield difference between TG-FTIR and lab scale pyrolysis is not as pronounced.

While a detailed comparison is hardly possible due to the strong feedstock dependency of the pyrolysis product spectrum, general observations in the literature are similar. Esperanza et al. [38] report CO and CO_2 as the predominant gaseous products of PUR varnish pyrolysis with yields of 8.9–18.0 mass-% and 5.6–16.6 mass-%, respectively. Veses et al. [20] report CO_2 yields of 6.2–11.6 mass-% from mattress foam waste pyrolysis. Garrido et al. [39] found CO_2 yields of 0.6–10.2 mass-% from viscoelastic memory foam pyrolysis. Although feedstock properties, experimental setups, and settings differ, the order of magnitude of the observed carbon dioxide yields is similar. This strongly hints at significant CO_2 formation as an intrinsic property of PUR pyrolysis.

Due to the high amounts of nitrogen in the investigated PUR, the potential formation of hydrogen cyanide (HCN) must be considered. HCN was not detected with the employed analytical equipment of this study and in previously reported analyses from TG-FTIR and Py-GC-MS [21, 22]. However, several studies report the formation of HCN from PUR pyrolysis. Eschenbacher et al. [32] have found no evidence of HCN formation in Py-GCxGC-MS of rigid and semirigid PUR at 400°C, 600°C, and 800°C. Garrido et al. [39] have not detected HCN at 550°C, while at pyrolysis temperatures of 650°C–850°C, a significant increase in HCN formation was evident. Similarly, a pronounced increase of HCN yields from 0.45 mass-% to 4.19 mass-% at temperatures of 700°C–800°C is reported by Grittner et al. [19]. From these literature references, an increasing probability of HCN formation with increased pyrolysis temperature can be derived. This is in accordance with the results of this study. No HCN was found. The presence of HCN in the pyrolysis gases of the experiments discussed above appears unlikely due to the low temperatures of 550°C and lower.

4 | Implications and Outlook for Chemical Recycling of PUR via Pyrolysis

In the context of chemical recycling, tight loops are beneficial to the recycling potential and the avoidance of environmental burdens. Therefore, the recovery of monomers is the preferred outcome of chemical recycling [14].

The element balances displayed in Figure 3 underline the heterogeneity of all pyrolysis products. Preferred migration of a certain element to a specific product phase is not evident. Therefore,

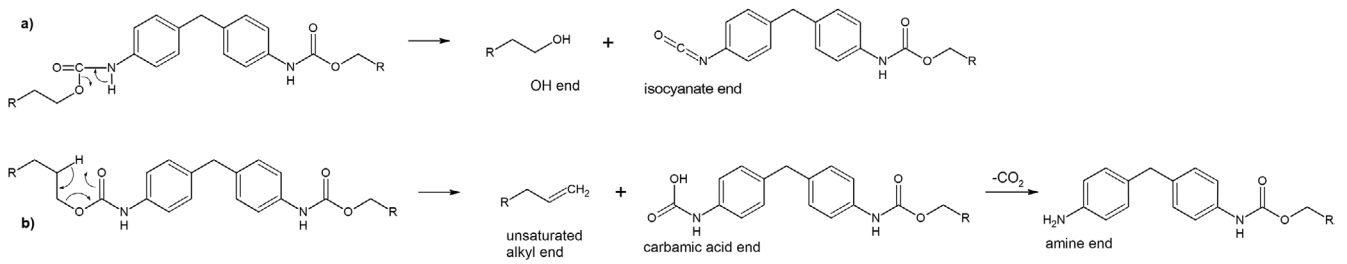

SCHEME 1 | Urethane bond scission mechanisms. Own illustration based on [17]

appropriate downstream processing must be developed for the utilization of the pyrolysis products. Py-GC-MS analyses have revealed the initial formation of MDI, the PUR monomer, during pyrolytic decomposition under ideal conditions [21]. Nevertheless, controlled depolymerization and recovery of the isocyanate monomer were demonstrated to be unfeasible in the lab-scale pyrolysis system. This implies that thermal pyrolysis, as performed in this work, does not yield products that can be applied in a polymer-to-polymer closed loop. Nonetheless, the amine derivative MDA forms as the predominant condensate compound. The formation of MDA and other aromatic amines, such as aniline and aminotoluene, originates from the urethane bond scission. The same scission mechanism also releases CO_2. In a recycling context, this is ambivalent. While high aromatic amine yields are desirable, the carbon bound in the released CO_2 is lost from a carbon circularity perspective. The maximum yield of amine products is roughly 15 mass-%, which are present in a mixture with diverse other condensed compounds. This implies the necessity of further purification for their recovery. Additionally, the majority of condensed products are lower-value compounds with a significant oxygen and nitrogen load. The solid yield is predominantly influenced by the pyrolysis temperature. From a technical viewpoint, the high-boiling products that are classified as solids in the presented experiment pose a risk. Even with residence times of several hours, no volatilization of these substances or cracking to compounds that volatilize at pyrolysis temperatures was achieved. As typical pyrolysis temperatures in commercial-scale plants lie around 500°C, accumulation in the system is to be expected. This might represent a significant constraint to the long-term operation of industrial-scale processes. Another aspect relevant to the large-scale operation of a PUR pyrolysis process and its integration into chemical industry value chains is the mitigation of toxic HCN release. Although the likelihood of HCN release from the investigated PUR at the discussed experimental settings is low, as discussed in Section 3.2.3, mitigation strategies must nevertheless be developed since even minor amounts of HCN can cause technical or safety problems. A multitude of promising approaches were gathered in a review by Chen et al. [40]. By catalyst application, a significant reduction of HCN in the pyrolysis gases is achievable.

As discussed above, closed-loop PUR-to-PUR polymer recycling is hardly feasible. In contrast, other recycling routes that aim for PUR recycling under a waste-to-chemicals premise appear more promising. Commonly discussed processes for pyrolysis condensates are hydrotreatment, steam cracking, and gasification. Hydrotreatment of PUR pyrolysis products would require a high hydrogen demand for heteroatom removal, substantial energy input, and suitable catalysts. For considering a pyrolysis condensate as a substitute feedstock in a steam cracker, the oxygen and nitrogen content must be below 100 ppm, respectively [24], which is far exceeded for PUR products. The N content in the condensates produced in the presented work ranges from 1.5% to 7.2%. Hence, the steam cracker recycling route for PUR pyrolysis products is not practical.

Gasification aims at the production of syngas by partial oxidation of the feedstock. The syngas mainly consists of CO, CO_2, H_2, and water. The high oxygen content of the pyrolysis condensate is therefore no hindrance. A further advantage of the gasification route is the additional utilization of the pyrolysis gas. This increases both the overall recycling rate and carbon recovery. Direct PUR gasification is reported and assessed positively in the literature [41, 42]. Nonetheless, denitrogenation of the syngas must be performed. In this context, Guo et al. [42] have identified CaO as a promising catalyst to mitigate HCN formation. Studies on combined pyrolysis and gasification of PUR are not known to the authors. The preceding pyrolysis step may serve to increase the energy density of the feedstock, improve feedstock dosing, and remove solid contaminants such as metals or mineral fillers. High-value pyrolysis products such as aniline or MDA may be recovered from the pyrolysis products, while the remaining product mixture is introduced into the gasifier. Hennig et al. [43] demonstrated the benefit of combined pyrolysis and gasification for complex mixed plastic waste from automotive recycling, including PUR. The technical feasibility, as well as the economic and ecological meaningfulness of combined pyrolysis and gasification for PUR recycling, are still to be investigated. In this regard, the results of the presented study lay the foundation for a thorough techno-economic assessment of pyrolysis as a recycling pathway to achieve circularity.

Author Contributions

Michael Zeller: conceptualization (lead), data curation (lead), formal analysis (lead), investigation (lead), methodology (lead), validation (lead), visualization (lead), writing – original draft (lead). **Lea Wattenberg:** data curation (supporting), formal analysis (supporting), investigation (supporting), validation (supporting), writing – review and editing (supporting). **Pratistha Shrestha:** data curation (supporting), formal analysis (supporting), investigation (supporting), methodology (supporting), validation (supporting). **Aylin Hannemann:** data curation (supporting), formal analysis (supporting), investigation (supporting), methodology (supporting), writing – review and editing (supporting). **Ankh-Erdene Erdenepurev:** data curation (supporting), formal analysis (supporting), investigation (supporting), methodology (supporting), writing – review and editing (supporting). **Niklas Netsch:** conceptualization (supporting), methodology (supporting), writing – review and editing (equal). **Britta Bergfeldt:** data curation

(supporting), formal analysis (supporting), methodology (supporting), resources (supporting), writing – review and editing (supporting). **Salar Tavakkol:** funding acquisition (equal), project administration (equal), resources (equal), supervision (equal), writing – review and editing (equal). **Dieter Stapf:** funding acquisition (lead), project administration (lead), resources (lead), writing – review and editing (equal).

Acknowledgments

The authors thank BASF Polyurethanes GmbH for the provision of the polyurethane samples. We also thank Monika Schleinkofer for the elemental analyses of the PUR and the pyrolysis products and Krassimir Garbev for assistance with the ATR-FTIR analysis. Open Access funding enabled and organized by Projekt DEAL.

The authors gratefully acknowledge funding of this study by the Helmholtz Association in the frame of the program "Materials and Technologies for the Energy Transition".

Funding

This work was supported by the Helmholtz Association (Program: Materials and Technologies for the Energy Transition).

Conflicts of Interest

The authors declare no conflicts of interest.

Data Availability Statement

Data will be made available upon reasonable request.

References

1. Independent Group of Scientists appointed by the Secretary-General, "Global Sustainable Development Report 2023: Times of crisis, times of change: Science for accelerating transformations to sustainable development," New York, 2023.

2. OECD, *Global Plastics Outlook: Policy Scenarios to 2060* (OECD Publishing, 2022).

3. K. Ragaert, L. Delva, and K. van Geem, "Mechanical and Chemical Recycling of Solid Plastic Waste," *Waste Management* 69 (2017): 24–58, https://doi.org/10.1016/j.wasman.2017.07.044.

4. European Commission, "Industrial Scale PET Chemical Recycling via an Innovative Glycolysis Process," accessed May 7, 2025, https://doi.org/10.3030/871386.

5. M. Laghezza, S. Fiore, and F. Berruti, "A Review on the Pyrolytic Conversion of Plastic Waste Into Fuels and Chemicals," *Journal of Analytical and Applied Pyrolysis* 179 (2024): 106479, https://doi.org/10.1016/j.jaap.2024.106479.

6. S. Kumagai, K. Fujiwara, T. Nishiyama, Y. Saito, and T. Yoshioka, "Chemical Feedstock Recovery Through Plastic Pyrolysis: Challenges and Perspectives Toward a Circular Economy," *ChemSusChem* 18 (2025): e2500210, https://doi.org/10.1002/cssc.202500210.

7. S. Chen and Y. H. Hu, "Advancements and Future Directions in Waste Plastics Recycling: From Mechanical Methods to Innovative Chemical Processes," *Chemical Engineering Journal* 493 (2024): 152727, https://doi.org/10.1016/j.cej.2024.152727.

8. PlasticsEurope, "Plastics - the fast Facts 2024," accessed May 7, 2025, https://plasticseurope.org/knowledge-hub/plastics-the-fast-facts-2024/.

9. G. Brereton, R. M. Emanuel, R. Lomax, et al., "Polyurethanes," in *Polyurethanes*, ed. G. Brereton, R. M. Emanuel, R. Lomax, et al. (Wiley-VCH Verlag GmbH & Co. KGaA, 2000), 1–76.

10. C. Lindner, J. Schmitt, J. Hein, and E. Fischer, "Stoffstrombild Kunststoffe in Deutschl 2023: Zahlen und Fakten zum Lebensweg von Kunststoffen," 2024.

11. G. Rossignolo, G. Malucelli, and A. Lorenzetti, "Recycling of Polyurethanes: Where We Are and Where We Are Going," *Green Chemistry* 26 (2024): 1132–1152, https://doi.org/10.1039/D3GC02091F.

12. M. M. Alavi Nikje, "Recycling of Polyurethane Wastes," in *Recycling of Polyurethane Wastes*, ed. M. M. Alavi Nikje (De Gruyter, 2019), V–VI.

13. D. Simón, A. M. Borreguero, A. de Lucas, and J. F. Rodríguez, "Glycolysis of Flexible Polyurethane Wastes Containing Polymeric Polyols," *Polymer Degradation and Stability* 109 (2014): 115–121, https://doi.org/10.1016/j.polymdegradstab.2014.07.009.

14. M. Pillich, J. Schilling, L. Bosetti, and A. Bardow, "What to Do With Polyurethane Waste? The Environmental Potential of Chemically Recycling Polyurethane Rigid Foam," *Green Chemistry* 26 (2024): 10893–10906, https://doi.org/10.1039/D4GC02594F.

15. M. Zeller, N. Netsch, F. Richter, H. Leibold, and D. Stapf, "Chemical Recycling of Mixed Plastic Wastes by Pyrolysis – Pilot Scale Investigations," *Chemie Ingenieur Technik* 93, no. 11 (2021): 1763–1770, https://doi.org/10.1002/cite.202100102.

16. J. Oenema, H. Liu, N. de Coensel, et al., "Review on the Pyrolysis Products and Thermal Decomposition Mechanisms of Polyurethanes," *Journal of Analytical and Applied Pyrolysis* 168 (2022): 105723, https://doi.org/10.1016/j.jaap.2022.105723.

17. S. Kumagai, S. Motokucho, R. Yabuki, et al., "Effects of Hard- and Soft-Segment Composition on Pyrolysis Characteristics of MDI, BD, and PTMG-Based Polyurethane Elastomers," *Journal of Analytical and Applied Pyrolysis* 126 (2017): 337–345, https://doi.org/10.1016/j.jaap.2017.05.012.

18. N. M. Mkhize, B. Danon, J. Alvarez, et al., "Influence of Reactor and Condensation System Design on Tyre Pyrolysis Products Yields," *Journal of Analytical and Applied Pyrolysis* 143 (2019): 104683, https://doi.org/10.1016/j.jaap.2019.104683.

19. N. Grittner, W. Kaminsky, and G. Obst, "Fluid Bed Pyrolysis of Anhydride-Hardened Epoxy Resins and Polyether-Polyurethane by the Hamburg Process," *Journal of Analytical and Applied Pyrolysis* 25 (1993): 293–299, https://doi.org/10.1016/0165-2370(93)80048-5.

20. A. Veses, O. Sanahuja-Parejo, I. Martínez, et al., "A Pyrolysis Process Coupled to a Catalytic Cracking Stage: A Potential Waste-To-Energy Solution for Mattress Foam Waste," *Waste Management* 120 (2021): 415–423, https://doi.org/10.1016/j.wasman.2020.09.052.

21. M. Zeller, K. Garbev, L. Weigel, et al., "Thermogravimetric Studies, Kinetic Modeling and Product Analysis of the Pyrolysis of Model Polymers for Technical Polyurethane Applications," *Journal of Analytical and Applied Pyrolysis* 171 (2023): 105976, https://doi.org/10.1016/j.jaap.2023.105976.

22. M. Zeller, D. Merz, L. Weigel, S. Tavakkol, and D. Stapf, "TG-FTIR Investigations of the Pyrolysis of Polyurethanes: Quantitative Carbon Dioxide Tracing, Decomposition Mechanisms, Products and Mass Balances for Advanced Recycling," *Journal of Analytical and Applied Pyrolysis* 188 (2025): 107048, https://doi.org/10.1016/j.jaap.2025.107048.

23. M. Zeller, S. Tavakkol, and D. Stapf, "Experimental and Analytical Tools for the Chemical Recycling of Engineering Plastics: A Multi-Scale Pyrolysis Study on Polydicyclopentadiene," *Macromolecular Rapid Communications* (2025): e2500161, https://doi.org/10.1002/marc.202500161.

24. M. Kusenberg, A. Eschenbacher, M. R. Djokic, et al., "Opportunities and Challenges for the Application of Post-Consumer Plastic Waste Pyrolysis Oils as Steam Cracker Feedstocks: To Decontaminate or Not to Decontaminate?," *Waste Management* 138 (2022): 83–115, https://doi.org/10.1016/j.wasman.2021.11.009.

25. J. Yu, L. Sun, C. Ma, Y. Qiao, and H. Yao, "Thermal Degradation of PVC: A Review," *Waste Management* 48 (2016): 300–314, https://doi.org/10.1016/j.wasman.2015.11.041.

26. M.-H. Cho, S.-H. Jung, and J.-S. Kim, "Pyrolysis of Mixed Plastic Wastes for the Recovery of Benzene, Toluene, and Xylene (BTX)

Aromatics in a Fluidized Bed and Chlorine Removal by Applying Various Additives," *Energy & Fuels* 24 (2010): 1389–1395, https://doi.org/10.1021/ef901127v.

27. J. Hubáček, J. Lederer, P. Kuráň, et al., "Dechlorination During Pyrolysis of Plastics: The Potential of Stepwise Pyrolysis in Combination With Metal Sorbents," *Fuel Processing Technology* 231 (2022): 107226, https://doi.org/10.1016/j.fuproc.2022.107226.

28. H. Günzler and H.-U. Gremlich, *IR-Spektroskopie: Eine Einführung* (Wiley-VCH GmbH & Co. KGaA, 2003).

29. B. A. Perez, J. V. J. Krishna, and H. E. Toraman, "Characterization of Polyolefins-Based Pyrolysis Oils: A Comparison Between One-Dimensional Gas Chromatography and Two-Dimensional Gas Chromatography," *Journal of Chromatography. A* 1739 (2025): 465510, https://doi.org/10.1016/j.chroma.2024.465510.

30. Y. Nishiyama, S. Kumagai, S. Motokucho, et al., "Temperature-Dependent Pyrolysis Behavior of Polyurethane Elastomers With Different Hard- and Soft-Segment Compositions," *Journal of Analytical and Applied Pyrolysis* 145 (2020): 104754, https://doi.org/10.1016/j.jaap.2019.104754.

31. M. Herrera, G. Matuschek, and A. Kettrup, "Thermal Degradation of Thermoplastic Polyurethane Elastomers (TPU) Based on MDI," *Polymer Degradation and Stability* 78 (2002): 323–331, https://doi.org/10.1016/S0141-3910(02)00181-7.

32. A. Eschenbacher, R. J. Varghese, J. Weng, and K. M. van Geem, "Fast Pyrolysis of Polyurethanes and Polyisocyanurate With and Without Flame Retardant: Compounds of Interest for Chemical Recycling," *Journal of Analytical and Applied Pyrolysis* 160 (2021): 105374, https://doi.org/10.1016/j.jaap.2021.105374.

33. R. P. Lattimer, "Mass Spectral Analysis of Low-Temperature Pyrolysis Products From Poly(Tetrahydrofuran)," *Journal of Analytical and Applied Pyrolysis* 57 (2001): 57–76, https://doi.org/10.1016/S0165-2370(00)00106-6.

34. H.-J. Hübschmann, *Handbuch der GC/MS: Grundlagen und Anwendung* (VCH, 1996).

35. H. Bockhorn, A. Hornung, U. Hornung, and D. Schawaller, "Kinetic Study on the Thermal Degradation of Polypropylene and Polyethylene," *Journal of Analytical and Applied Pyrolysis* 48 (1999): 93–109, https://doi.org/10.1016/S0165-2370(98)00131-4.

36. L. Cheng, J. Gu, Y. Wang, J. Zhang, H. Yuan, and Y. Chen, "Polyethylene High-Pressure Pyrolysis: Better Product Distribution and Process Mechanism Analysis," *Chemical Engineering Journal* 385 (2020): 123866, https://doi.org/10.1016/j.cej.2019.123866.

37. L. Costa, M. P. Luda, G. G. Cameron, and M. Y. Qureshi, "The Thermal and Thermo-Oxidative Degradation of Poly(Tetrahydrofuran) and Its Complexes With LiBr and LiI," *Polymer Degradation and Stability* 67 (2000): 527–533, https://doi.org/10.1016/S0141-3910(99)00154-8.

38. M. M. Esperanza, A. N. García, R. Font, and J. A. Conesa, "Pyrolysis of Varnish Wastes Based on a Polyurethane," *Journal of Analytical and Applied Pyrolysis* 52 (1999): 151–166, https://doi.org/10.1016/S0165-2370(99)00048-0.

39. M. A. Garrido, R. Font, and J. A. Conesa, "Pollutant Emissions From the Pyrolysis and Combustion of Viscoelastic Memory Foam," *Science of the Total Environment* 577 (2017): 183–194, https://doi.org/10.1016/j.scitotenv.2016.10.159.

40. G. Chen, T. Liu, P. Luan, et al., "Distribution, Migration, and Removal of N-Containing Products During Polyurethane Pyrolysis: A Review," *Journal of Hazardous Materials* 453 (2023): 131406, https://doi.org/10.1016/j.jhazmat.2023.131406.

41. W.-S. Yang, J.-S. Lee, S.-W. Park, J.-J. Kang, T. Alam, and Y.-C. Seo, "Gasification Applicability Study of Polyurethane Solid Refuse Fuel Fabricated From Electric Waste by Measuring Syngas and Nitrogenous Pollutant Gases," *Journal of Material Cycles and Waste Management* 18 (2016): 509–516, https://doi.org/10.1007/s10163-016-0512-1.

42. X. Guo, W. Zhang, L. Wang, and J. Hao, "Comparative Study of Nitrogen Migration Among the Products From Catalytic Pyrolysis and Gasification of Waste Rigid Polyurethane Foam," *Journal of Analytical and Applied Pyrolysis* 120 (2016): 144–153, https://doi.org/10.1016/j.jaap.2016.04.018.

43. M. Hennig, T. Dreising, A. Reeves, et al., "Entrained-Flow Gasification for the Utilization of Pyrolysis Oil From Mixed Plastic Waste," *ACS Sustainable Chemistry & Engineering* (2025).

Supporting Information

Additional supporting information can be found online in the Supporting Information section. **Data S1:** Supplementary Information.